Chapter 3
Dynamics

3.1 Introduction to Dynamical Systems

Dynamical systems theory provides a powerful tool for analyzing nonlinear systems of differential equations, including those that arise in neuroscience. This theory allows us to interpret solutions geometrically as curves in a phase space. By studying the geometric structure of phase space, we are often able to classify the types of solutions that a model may exhibit and determine how solutions depend on the model's parameters. For example, we can often predict if a model neuron will generate an action potential, determine for which values of the parameters the model will produce oscillations, and compute how the frequency of oscillations depends on the parameters.

In this chapter, we introduce many of the basic concepts of dynamical systems theory using a reduced two-variable model: the Morris–Lecar equations. Although this model is considerably simpler than the Hodgkin–Huxley equations, it still exhibits many important features of neuronal activity. For example, the Morris–Lecar model generates action potentials, there is a threshold for firing, and the model displays sustained oscillations at elevated levels of an applied current. By considering a reduced model, we can more easily explain the geometric mechanisms underlying each of these phenomena. Moreover, we can introduce important mathematical concepts such as phase space analysis, bifurcation theory, oscillations, and stability theory. Each of these concepts plays a fundamental role in the analysis of more complex systems discussed throughout the book.

3.2 The Morris–Lecar Model

One of the simplest models for the production of action potentials is a model proposed by Kathleen Morris and Harold Lecar. The model has three channels: a potassium channel, a leak, and a calcium channel. In the simplest version of

G.B. Ermentrout and D.H. Terman, *Mathematical Foundations of Neuroscience*, Interdisciplinary Applied Mathematics 35, DOI 10.1007/978-0-387-87708-2_3,

the model, the calcium current depends instantaneously on the voltage. Thus, the Morris–Lecar equations have the form

$$\begin{aligned} C_{\mathrm{M}}\frac{\mathrm{d}V}{\mathrm{d}t} &= I_{\mathrm{app}} - g_{\mathrm{L}}(V - E_{\mathrm{L}}) - g_{\mathrm{K}}n(V - E_{\mathrm{K}}), \\ &\quad -g_{\mathrm{Ca}}m_{\infty}(V)(V - E_{\mathrm{Ca}}) \;\equiv\; I_{\mathrm{app}} - I_{\mathrm{ion}}(V, n), \\ \frac{\mathrm{d}n}{\mathrm{d}t} &= \phi(n_{\infty}(V) - n)/\tau_n(V), \end{aligned} \tag{3.1}$$

where

$$\begin{aligned} m_{\infty}(V) &= \frac{1}{2}[1 + \tanh((V - V_1)/V_2)], \\ \tau_n(V) &= 1/\cosh((V - V_3)/(2V_4)), \\ n_{\infty}(V) &= \frac{1}{2}[1 + \tanh((V - V_3)/V_4)]. \end{aligned}$$

Here, V_1, V_2, V_3, and V_4 are parameters chosen to fit voltage-clamp data.

The solutions shown in Fig. 3.1 demonstrate that the Morris–Lecar model exhibits many of the properties displayed by neurons. Here, the parameters are listed in Table 3.1 under the Hopf case. Figure 3.1a demonstrates that the model is *excitable* if $I_{\mathrm{app}} = 60$. That is, there is a stable constant solution corresponding to the resting state of the model neuron. A small perturbation decays to the resting state, whereas a larger perturbation, above some threshold, generates an action potential. The solution $(V_1(t), n_1(t)) \equiv (V_{\mathrm{R}}, n_{\mathrm{R}})$ is constant; V_{R} is the resting state of the model neuron. The solution $(V_2(t), n_2(t))$ corresponds to a subthreshold response. Here, $V_2(0)$ is slightly larger than V_{R} and $(V_2(t), n_2(t))$ decays back to rest. Finally,

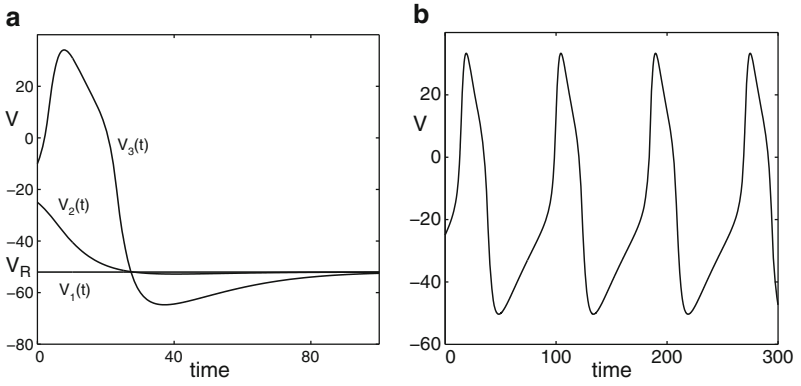

Fig. 3.1 Solutions of the Morris–Lecar equations. Parameters are listed in Table 3.1, the Hopf case. (**a**) A small perturbation from rest decays to the resting state, whereas a larger perturbation generates an action potential. Here, $I_{\mathrm{app}} = 60$. (**b**) A periodic solution of the Morris–Lecar equations. Here, $I_{\mathrm{app}} = 100$

Table 3.1 Morris–Lecar parameters; the current, I_{app}, is a parameter

Parameter	Hopf	SNLC	Homoclinic
ϕ	0.04	0.067	0.23
g_{Ca}	4.4	4	4
V_3	2	12	12
V_4	30	17.4	17.4
E_{Ca}	120	120	120
E_{K}	−84	−84	−84
E_{L}	−60	−60	−60
g_{K}	8	8	8
g_{L}	2	2	2
V_1	−1.2	−1.2	−1.2
V_2	18	18	18
C_{M}	20	20	20

SNLC saddle–node on a limit cycle

$(V_3(t), n_3(t))$ corresponds to an action potential. Here, we start with $V_3(0)$ above some threshold. There is then a large increase of $V_3(t)$, followed by $V_3(t)$ falling below V_{R} and then a return to rest.

Figure 3.1b shows a periodic solution of the Morris–Lecar equations. The parameter values are exactly the same as before; however, we have increased the parameter I_{app}, corresponding to the applied current. If we increase I_{app} further, then the frequency of oscillations increases; if I_{app} is too large, then the solution approaches a constant value.

In the following, we will show how dynamical systems methods can be used to mathematically analyze these solutions. The analysis is extremely useful in understanding when this type of model, for a given set of parameters, displays a particular type of behavior. The behavior may change as parameters are varied; an important goal of bifurcation theory, which we describe later, is to determine when and what types of transitions take place. Our introduction to dynamical systems will be brief and we will only discuss those topics needed for the rest of the book. Readers interested in learning more about dynamical systems should consult one of the books listed in Sect. 3.8.

3.3 The Phase Plane

It will be convenient to write (3.1) as

$$\begin{aligned} \frac{\mathrm{d}V}{\mathrm{d}t} &= f(V,n), \\ \frac{\mathrm{d}n}{\mathrm{d}t} &= g(V,n). \end{aligned} \tag{3.2}$$

The phase space for this system is simply the (V, n) plane; this is usually referred to as the *phase plane*. If $(V(t), n(t))$ is a solution of (3.2), then at each time t_0, $(V(t_0), n(t_0))$ defines a point in the phase plane. The point changes with time, so the entire solution $(V(t), n(t))$ traces out a curve (or trajectory or orbit) in the phase plane.

Of course, not every arbitrarily drawn curve in the phase plane corresponds to a solution of the differential equations. What is special about solution curves is that the velocity vector at each point along the curve is given by the right-hand side of (3.2). That is, the velocity vector of the solution curve $(V(t), n(t))$ at a point (V_0, n_0) is given by $(V'(t), n'(t)) = (f(V_0, n_0), g(V_0, n_0))$. This geometric property – that the vector $(f(V, n), g(V, n))$ always points in the direction that the solution is flowing – completely characterizes the solution curves.

Two important types of trajectories are *fixed points* (sometimes called *equilibria* or *rest points*) and *closed orbits*. At a fixed point, $f(V_\mathrm{R}, n_\mathrm{R}) = g(V_\mathrm{R}, n_\mathrm{R}) = 0$; this corresponds to a constant solution. Closed orbits correspond to periodic solutions. That is, if $(v(t), n(t))$ represents a closed orbit, then there exists $T > 0$ such that $(V(t), n(t)) = (V(t + T), n(t + T))$ for all t.

A useful way to understand how trajectories behave in the phase plane is to consider the *nullclines*. The V-nullcline is the curve defined by $V' = f(V, n) = 0$ and the n-nullcline is where $n' = g(V, n) = 0$. Note that along the V-nullcline, the vector field $(f(V, n), g(V, n))$ points either up or down, and along the n-nullcline, vectors point either to the left or to the right. Fixed points are where the two nullclines intersect. The nullclines divide the phase plane into separate regions; in each of these regions, the vector field points in the direction of one of the four quadrants: (1) $f > 0,\ g > 0$; (2) $f < 0,\ g > 0$; (3) $f < 0,\ g < 0$; or (4) $f > 0,\ g < 0$.

3.3.1 Stability of Fixed Points

One can determine the stability of a fixed point by considering the linearization of the vector field at the fixed point. The linearization of (3.2) at a fixed point $(V_\mathrm{R}, n_\mathrm{R})$ is the matrix

$$M = \begin{bmatrix} \dfrac{\partial f}{\partial V}(V_\mathrm{R}, n_\mathrm{R}) & \dfrac{\partial f}{\partial n}(V_\mathrm{R}, n_\mathrm{R}) \\ \dfrac{\partial g}{\partial V}(V_\mathrm{R}, n_\mathrm{R}) & \dfrac{\partial g}{\partial n}(V_\mathrm{R}, n_\mathrm{R}) \end{bmatrix}.$$

The fixed point is stable if both of the eigenvalues of this matrix have a negative real part; the fixed point is unstable if at least one of the eigenvalues has a positive real part. For the Morris–Lecar equations, the linearization is given by

$$M = \begin{bmatrix} -\dfrac{\partial I_\mathrm{ion}(V_\mathrm{R}, n_\mathrm{R})}{\partial V}/C_\mathrm{M} & -g_\mathrm{K}(V_\mathrm{R} - E_\mathrm{K})/C_\mathrm{M} \\ \phi n'_\infty(V_\mathrm{R})/\tau_n(V_\mathrm{R}) & -\phi/\tau_n(V_\mathrm{R}) \end{bmatrix} \equiv \begin{bmatrix} a & b \\ c & d \end{bmatrix}.$$

Moreover,

$$a \equiv -\frac{\partial I_{\text{ion}}(V_{\text{R}}, n_{\text{R}})}{\partial V} \Big/ C_{\text{M}}$$
$$= (-g_{\text{L}} - g_{\text{K}} n_{\text{R}} - g_{\text{Ca}} m_{\infty}(V_{\text{R}}) + (E_{\text{Ca}} - V_{\text{R}}) g_{\text{Ca}} m'_{\infty}(V_{\text{R}}))/C_{\text{M}}.$$

We now find conditions on the nonlinear functions in (3.1) for when the fixed point is stable.

Suppose the equilibrium voltage lies between E_{K} and E_{Ca}, a reasonable assumption. Then $b < 0$, $c > 0$, and $d < 0$ in the linearization. Only a can be either negative or positive and the only term contributing to the positivity of a is the slope of the calcium activation function, $m_{\infty}(V)$. If $a < 0$, then the fixed point is asymptotically stable since the trace of M is negative and the determinant is positive. (Recall that the trace is the sum of the eigenvalues and the determinant is the product of the eigenvalues.) Note that the slope of the V-nullcline near the fixed point is given by $-a/b$. Since $b < 0$, it follows that if this slope is negative, then the fixed point is stable; that is, if the fixed point lies along the left branch of the V-nullcline, then it is stable (see Fig. 3.2).

Now suppose the fixed point lies along the middle branch of the V-nullcline, so $a > 0$. Note that the slope of the n-nullcline, $-c/d$, is always positive. If the slope of the V-nullcline is greater than the slope of the n-nullcline (i.e., $-a/b > -c/d$), then $ad - bc < 0$. In this case, the determinant is negative and the fixed point is an unstable saddle point. In contrast, if the slope of the n-nullcline is greater than that of the V-nullcline, then the fixed point is a node or a spiral. In this case, the stability of the fixed point is determined by the trace of M: the fixed point is stable if $a + d < 0$ and it is unstable if $a + d > 0$. Since $a > 0$ and $d = -\phi/\tau_n(V_{\text{R}})$, it follows that the fixed point is unstable if ϕ is sufficiently small. Note that ϕ governs the speed of the potassium dynamics.

3.3.2 *Excitable Systems*

Recall that for the parameters given in Table 3.1 for the Hopf case, the system is *excitable* if $I_{\text{app}} = 60$. As Fig. 3.1a demonstrates, a small perturbation in voltage from the resting state decays back to rest, whereas a sufficiently large perturbation in voltage continues to increase and generates an action potential.

Phase plane analysis is very useful for understanding what separates the firing of an action potential from the subthreshold return to rest in this model. The projection of the solutions shown in Fig. 3.1a onto the phase plane are shown in Fig. 3.2a. This figure also shows the V-nullcline and the n-nullcline. Note that the V-nullcline separates points along trajectories in which $V' < 0$ and $V' > 0$. In particular, V increases below the V-nullcline and V decreases above the V-nullcline. We further note that the V-nullcline is "cubic." This suggests a perturbation from rest that lies to the "left" of the middle branch of the V-nullcline will return quickly to rest, whereas

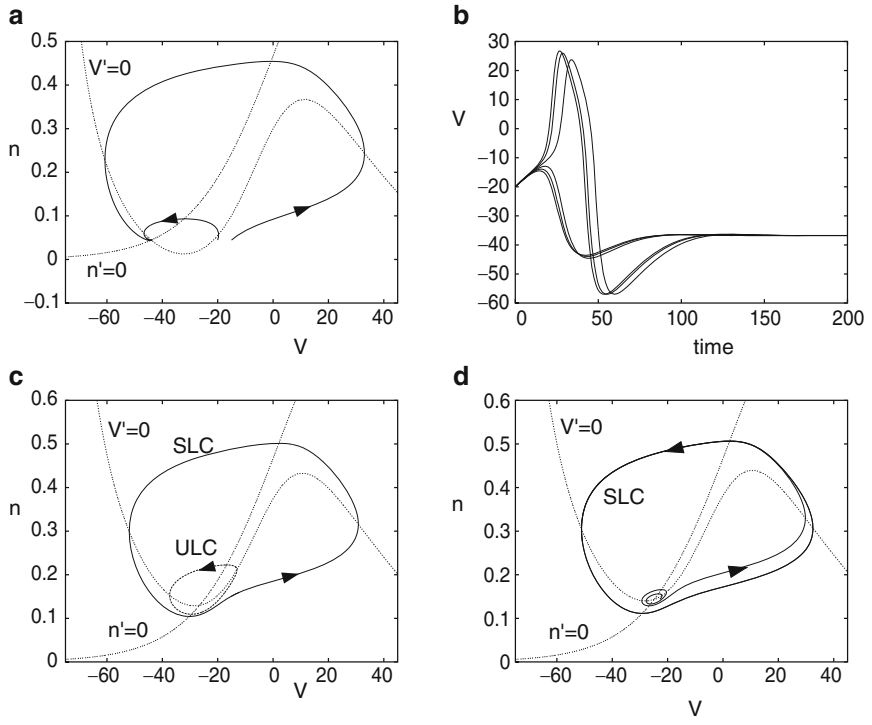

Fig. 3.2 Phase planes and voltage traces for the Morris–Lecar model in the Hopf regime. (**a**) $I_{\text{app}} = 60$; an excitable system with threshold at about -20 mV. Nullclines are included as well. (**b**) Starting at $n = n_{\text{rest}}$ and varying V from -20 to -20.1 mV leads to graded action potentials. (**c**) $I_{\text{app}} = 90$ showing bistability between a stable limit cycle (*SLC*) and a fixed point, separated by the unstable limit cycle (*ULC*). (**d**) $I_{\text{app}} = 100$, the fixed point is unstable and only a limit cycle remains

a perturbation that lies to the "right" of the middle branch of the V-nullcline will initially display an increase in membrane potential, corresponding to an action potential, before returning to rest. Therefore, the middle branch of the V-nullcline in some sense separates the firing of an action potential from the subthreshold return to rest.

This analysis can be made more precise if we assume the parameter ϕ is small. Looking at Table 3.1, we can see that ϕ is relatively smaller in the Hopf case than in the other two cases. For small ϕ, n will not change much, so let us hold it at rest. Figure 3.3 shows the phase plane with a horizontal line drawn through the fixed point. If n does not change much, then the dynamics are governed by the behavior on the phase line $n = n_{\text{R}}$. Since the V-nullcline intersects this line at three points, there are three equilibria for the system when n is held constant. The resting state (and true equilibrium of the full system) V_{R} is stable. There are two additional equilibria (which are not equilibria of the full model, just the model when n is held at its resting value): V_θ, which is unstable, and V_{e}, which is stable. On this line, if the voltage is

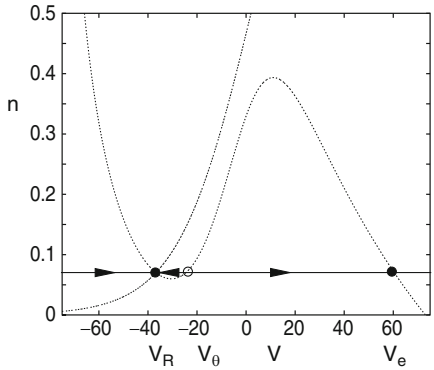

Fig. 3.3 Threshold construction for the Morris–Lecar model

perturbed past V_θ, then it will jump to the right fixed point, V_e. Otherwise, it will decay to rest, V_R. This shows that for small ϕ, the "threshold" voltage for generating an action potential is roughly the intersection of the horizontal line through the resting state and the middle branch of the V-nullcline. Since experimentalists can only move the voltage through current injection, we can use this to estimate the magnitude of a current pulse needed to cross the threshold (see Exercise 2).

We note that the peak of the action potential occurs at some latency after the initial perturbation, but this latency can never become very large. The action potential itself is graded and takes on a continuum of peak values, as shown in Fig. 3.2b. If ϕ is not "small" and it is increased, then the spike amplitudes are even more graded than those shown in Fig. 3.2b. Recall that ϕ is related to the temperature of the preparation. Thus, increasing the temperature of a neuron should lead to a much less sharp threshold distinction and graded action potentials. Indeed, Cole et al. [42] demonstrated this in the squid axon.

3.3.3 Oscillations

We expect the phase plane to change if a parameter in the equations changes. Figure 3.2d shows the phase plane corresponding to the periodic solution shown in Fig. 3.1b. Here, $I_\mathrm{app} = 100$. Note that the periodic solution corresponds to a closed curve or *limit cycle*. In general, whenever we wish to find periodic solutions of some model, we look for closed orbits in phase space. In Fig. 3.2d, there is a unique fixed point; this is where the nullclines intersect. This fixed point is unstable, however.

If we change I_app to 90, then the model is *bistable*, and the phase plane is shown in Fig. 3.2c. Note that there exist both a stable fixed point and a stable limit cycle. Small perturbations from rest will decay back to the stable fixed point, whereas large perturbations will approach the stable periodic solution. Note that there also exists an unstable periodic solution. This orbit separates those initial conditions that approach the stable fixed point from those that approach the stable limit cycle.

It is often difficult to show that a given model exhibits stable oscillations, especially in higher-dimensional systems such as the Hodgkin–Huxley model. Limit cycles are global objects, unlike fixed points, which are local. To demonstrate that a given point is on a periodic solution, one must follow the trajectory passing through that point and wait to see if the trajectory returns to where it started. This is clearly not a useful strategy for finding periodic solutions. A powerful method for locating oscillatory behavior is bifurcation theory, which we describe in Sect. 3.4.

3.4 Bifurcation Analysis

Bifurcation theory is concerned with how solutions change as parameters in a model are varied. For example, in the previous section we showed that the Morris–Lecar equations may exhibit different types of solutions for different values of the applied current I_{app}. If $I_{\text{app}} = 60$, then there is a stable fixed point and no oscillations, whereas if $I_{\text{app}} = 100$, then the fixed point is unstable and a stable limit cycle exists. Using bifurcation theory, we can classify the types of transitions that take place as we change parameters. In particular, we can predict for which value of I_{app} the fixed point loses its stability and oscillations emerge. There are, in fact, several different types of bifurcations; that is, there are different mechanisms by which stable oscillations emerge. The most important types of bifurcations can be realized by the Morris–Lecar model. These are described next.

3.4.1 The Hopf Bifurcation

In Fig. 3.4, we chose the parameters as in Table 3.1 for the Hopf regime and show the *bifurcation diagram* for the Morris–Lecar equations as I_{app} is varied. For each value of I_{app}, there is a unique fixed point, $(V_{\text{R}}(I_{\text{app}}), n_{\text{R}}(I_{\text{app}}))$. In Fig. 3.4a, we plot V_{R} versus I_{app}. The fixed point is stable for $I_{\text{app}} < 94 \equiv I_1$ and $I_{\text{app}} > 212 \equiv I_2$; otherwise, it is unstable. A *Hopf bifurcation* occurs at $I_{\text{app}} = I_1$ and $I_{\text{app}} = I_2$. By this we mean the following. Recall that a fixed point is stable if all of the eigenvalues of the linearization have a negative real part; the fixed point is unstable if at least one of the eigenvalues has a positive real part. The fixed point loses stability, as a parameter is varied, when at least one eigenvalue crosses the imaginary axis. If the eigenvalues are all real numbers, then they can cross the imaginary axis only at the origin in the complex plane. However, if an eigenvalue is complex, then it (and its complex conjugate) will cross the imaginary axis at some point that is not at the origin. This latter case corresponds to the Hopf bifurcation and it is precisely what happens for the example we are considering. In this example, $(I_1, V_{\text{R}}(I_1), n_{\text{R}}(I_1))$ and $(I_2, V_{\text{R}}(I_2), n_{\text{R}}(I_2))$ are called *bifurcation points*. Sometimes, I_1 and I_2 are also referred to as bifurcation points. The *Hopf bifurcation theorem* states that (if certain technical assumptions are satisfied) there must exist values of the parameter I_{app}

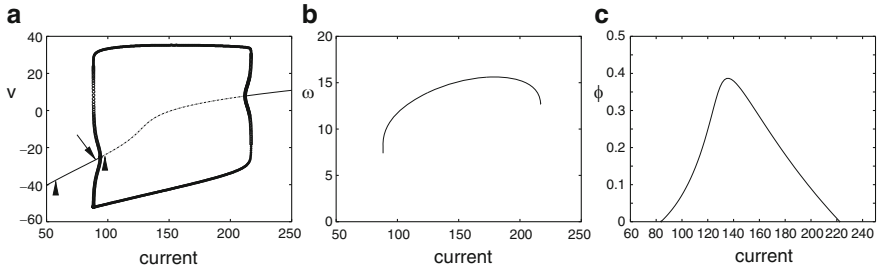

Fig. 3.4 Bifurcation diagram for the Morris–Lecar model in the Hopf regime. (**a**) Voltage as a function of current. The *curves* above and below the fixed-point curve correspond to the maximum and minimum voltages along periodic orbits. *Solid curves* represent stable solutions and *dashed curves* represent unstable solutions. *Arrows* shown at $I_{\text{app}} = 60, 90,$ and 100 correspond to the solutions shown in Fig. 3.2a, c, and d, respectively. (**b**) Frequency (Hz) versus current. (**c**) Two-parameter bifurcation showing the curve of Hopf bifurcations as ϕ and I_{app} vary

near I_1 and I_2 such that there exist periodic solutions that lie near the fixed points $(V_{\text{R}}(I_{\text{app}}), n_{\text{R}}(I_{\text{app}}))$. A more precise statement of the Hopf bifurcation theory can be found in numerous texts on dynamical systems.

The curves in Fig. 3.4a represent fixed points and periodic solutions of the Morris–Lecar model. This diagram was generated using the numerical software program XPPAUT. The curve above the fixed-point curve represents the maximum voltages on the periodic orbits and the curve below the fixed-point curve represents the minimum voltages. The solid curves represent stable solutions and the dashed curves represent unstable solutions. The bifurcation diagram shows many interesting and important features. Note that the periodic solutions near the two bifurcation points are unstable. These unstable, small-amplitude periodic solutions lie on the same side of the bifurcation points as the stable fixed points. These are both examples of *subcritical Hopf bifurcations*. At a *supercritical Hopf bifurcation*, the small-amplitude periodic solutions near the Hopf bifurcation point are stable and lie on the side opposite the branch of stable fixed points.

If $88.3 < I_{\text{app}} < I_1$ or $I_2 < I_{\text{app}} < 217$, then the Morris–Lecar model is bistable. For these values of I_{app}, there exist both a stable fixed point and a stable periodic solution. The phase plane for $I_{\text{app}} = 90$ is shown in Fig. 3.2c. Note that small perturbations of initial conditions from the resting state will decay back to rest; however, large perturbation from rest will generate solutions that approach the stable limit cycles.

Figure 3.4b shows the frequency of the stable periodic solutions versus current. Note that the frequency lies in a narrow range between 7 and 16 Hz. In particular, the frequency does not approach zero as I_{app} approaches the bifurcation points. This is a general property of periodic solutions that arise via the Hopf bifurcation. In Sect. 3.4.2, we shall consider another mechanism for the generation of stable limit cycles. In that mechanism, the frequency does approach zero.

Finally, we can ask what happens if we change the speed of the potassium kinetics. Figure 3.4c shows a two-parameter diagram with ϕ along the vertical axis and

I_{app} along the horizontal axis. This shows the locus of Hopf bifurcations in these two parameters. For fixed values of ϕ below about 0.4, there are two currents at which the Hopf bifurcation occurs. Inside the curve, the resting state is unstable. One can numerically show that the Hopf bifurcation is subcritical outside the interval $124.47 < I_{\text{app}} < 165.68$; inside this interval, the bifurcation is supercritical. The reader can choose, for example, $\phi = 0.35$ and show that both Hopf bifurcations are supercritical; the only oscillations are stable and have small amplitude.

3.4.2 Saddle–Node on a Limit Cycle

The Hopf bifurcation is the best known mechanism through which one can go from a stable fixed point to an oscillation. Importantly, the fixed point persists through the bifurcation. Furthermore, the limit cycles which bifurcate are of *small amplitude* and are local, in the sense that they lie close to the branch of fixed points (although, as we saw in the Morris–Lecar model, the bifurcation is subcritical at low currents and thus bifurcating periodic orbits are unstable). Another mechanism through which an oscillation can emerges from a fixed point is called a *saddle–node on a limit cycle* (SNLC). It is also called a *saddle–node on an invariant circle* (SNIC). This is an example of a global bifurcation.

The behavior of the Morris–Lecar model with these parameters is quite different, as is shown in Fig. 3.5. First, unlike in Fig. 3.2b, the action potentials appear to occur with arbitrary delay after the end of the stimulus. Second, the shape of the action potentials is much less variable. The reason for this can be understood by looking at the phase plane in Fig. 3.5b. Unlike the Hopf case, here there are three fixed points, only one of which (labeled N) is stable. The middle fixed point is a saddle point (labeled S). Thus, the linearized system at this fixed point has one positive and one negative eigenvalue. Associated with these eigenvalues are the stable and unstable manifolds. These manifolds consist of trajectories that approach the saddle point in either forward or backward time, respectively. The two branches of the unstable manifold, Σ^+, form a loop with the stable node N and the saddle point S. This loop in the plane constrains the spike shape; since trajectories cannot cross, any trajectory starting outside the loop must remain outside it. Thus, the spike height cannot fall below a certain level. More importantly, the stable manifold, Σ^-, forms a hard threshold that is precisely determined. This contrasts with the pseudothreshold we saw in the Hopf case. Any perturbation which drives the potential to the right of Σ^- results in a spike and any perturbation which drives the potential to the left of Σ^- leads to a return to rest without a spike.

Figure 3.5 also explains the delay in firing. Suppose a stimulus drives the voltage to a point exactly on the stable manifold Σ^-. Then, the trajectory will go to the saddle point, where it will remain. The closer a perturbation gets to Σ^- (but to the right of it), the longer the delay to the spike. Indeed, the spike with the longest delay in Fig. 3.5a stays at a nearly constant voltage close to the value at the saddle point before finally firing.

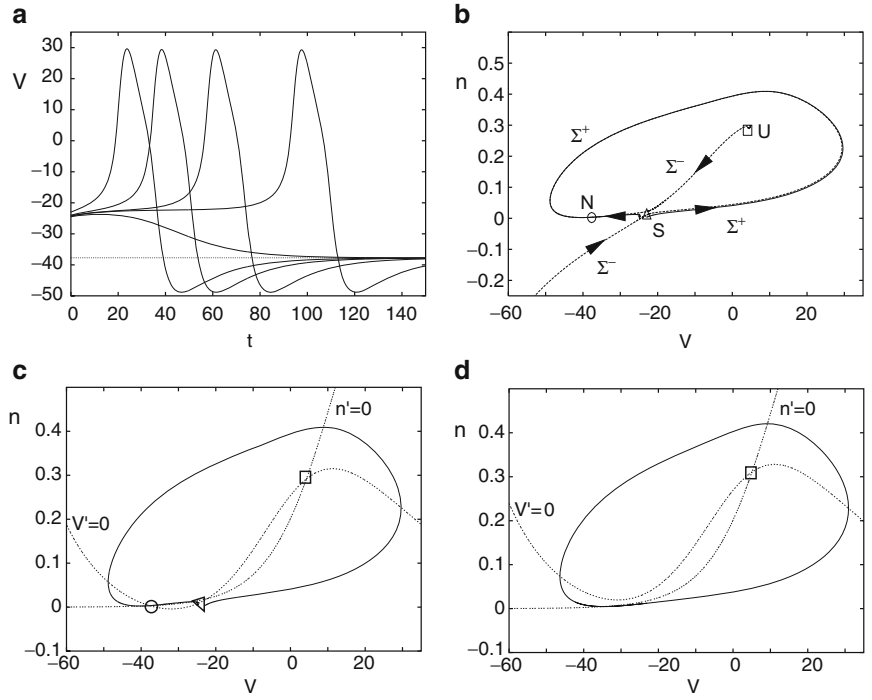

Fig. 3.5 Dynamics of the Morris–Lecar model with saddle–node dynamics. (**a**) The delay to spiking can be arbitrary but the spike height is invariant. For the different plots, we start with different initial conditions. (**b**, **c**) Phase plane explaining (**a**). The fixed points N, S, and U are, respectively a stable node (the resting state), a saddle point, and an unstable node. $\Sigma^{\pm}$ are the stable $(-)$ and unstable $(+)$ manifolds of S. (**d**) There exists a stable limit cycle for sufficient current; the nullclines are also shown

Like the Hopf case, as current is increased, the model fires repetitively. A typical limit cycle is shown in Fig. 3.5d. Figure 3.6a shows the bifurcation diagram as the current is increased. The steady-state voltage shows a region where there are three equilibria for I_{app} between about -15 and $+40$. Only the lower fixed point is stable. As I_{app} increases, the saddle point and the stable node merge together at a saddle–node bifurcation, labeled SN_2. When $I_{\text{app}} = I_{\text{SN}_2}$, the invariant loop formed from Σ^+ becomes a homoclinic orbit; that is, it is a single trajectory that approaches a single fixed point in both forward and backward time. This type of homoclinic orbit is sometimes called a *saddle–node homoclinic orbit* or a SNIC. As I_{app} increases past $I_{\text{app}} = I_{\text{SN}_2}$, the saddle point and node disappear; the invariant loop formed from Σ^+ becomes a stable limit cycle. The branch of limit cycles persists until it meets a branch of unstable periodic solutions emerging from a subcritical Hopf bifurcation.

Figure 3.6b shows the frequency of the oscillations as a function of the current. Unlike in Fig. 3.4b, the frequency for this model can be arbitrarily low and there is a

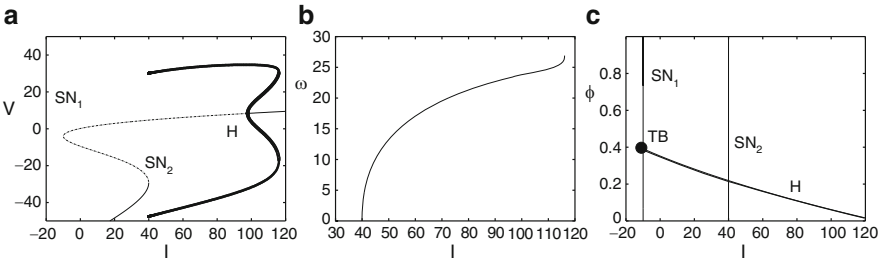

Fig. 3.6 Bifurcation for the Morris–Lecar model with saddle–node dynamics. (**a**) Voltage versus current showing saddle–node (SN_1, SN_2) and Hopf (H) bifurcations. (**b**) Frequency as a function of current. (**c**) Two-parameter bifurcation diagram showing the curves of Hopf and saddle–node bifurcations as the rate, ϕ, of the potassium channel varies. The Hopf curve meets the leftmost saddle–node curve at a double-zero eigenvalue characterizing a Takens–Bogdanov bifurcation (TB)

much greater dynamic range. Note that the nullclines in Fig. 3.5c can be very close to touching each other and thus create a narrow channel where the flow is extremely slow. This suggests why the frequency of firing can be arbitrarily low. Moreover, as $I_{\text{app}} \to I_{\text{SN}_2}$, the limit cycles approach a homoclinic orbit. We expect that the frequency should approach zero as $I_{\text{app}} \to I_{\text{SN}_2}$. In an exercise later, the reader is asked to show that the frequency scales as the square root of $I_{\text{app}} - I_{\text{SN}_2}$ and to develop the theta model.

3.4.3 Saddle–Homoclinic Bifurcation

By changing the rate of the potassium channel, ϕ, we can alter the dynamics of the model so that the SNIC is replaced by another type of global bifurcation; this is called a *saddle–homoclinic bifurcation*. In both types of bifurcations, the frequency of oscillations approaches zero as the current approaches the bifurcation value. However, there are important differences.

Since ϕ only changes the rate of n, it has no effect on the number and values of the fixed points, only their stability. Figure 3.7 shows the bifurcation diagram for the model when ϕ is increased from 0.067 to 0.23. As before, the fixed points are lost at a saddle–node bifurcation. The Hopf bifurcation on the upper branch occurs at a much lower value of current than in Fig. 3.6, but the Hopf bifurcation is still subcritical. The main difference is that the stable branch of periodic orbits does not terminate on the saddle–node as in Fig. 3.6. Rather it terminates on an orbit that is homoclinic to one of the saddle points along the middle branch of fixed points. Like the SNIC, this homoclinic orbit has an infinite period. However, the periods of the limit cycles approach infinity quite differently from before. One can show that the period scales as

$$T \sim \ln \frac{1}{I_{\text{app}} - I_{\text{Hc}}},$$

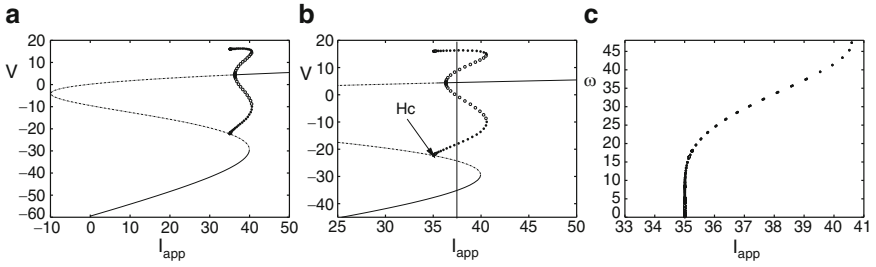

Fig. 3.7 Bifurcation for the Morris–Lecar model with increased ϕ. (**a**) Voltage versus current. (**b**) Zoom in of (**a**) showing the homoclinic orbit (*Hc*). The *vertical line* at $I_{\text{app}} = 37$ shows tristability. (**c**) Frequency versus current; note the much steeper approach to I^* than in Fig. 3.6

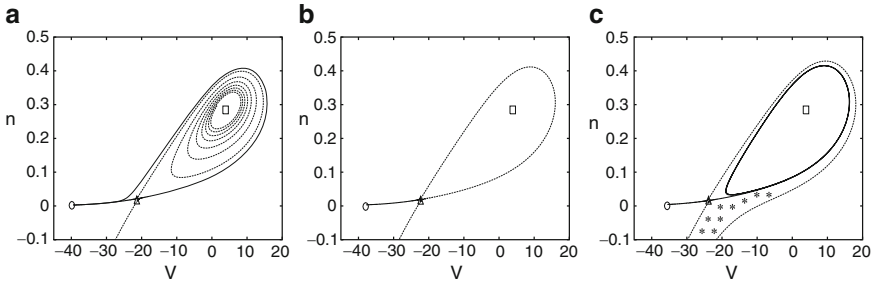

Fig. 3.8 Phase plane for the Morris–Lecar system near the homoclinic bifurcation showing (**a**) $I_{\text{app}} < I_{\text{Hc}}$, (**b**) $I_{\text{app}} \approx I_{\text{Hc}}$, and (**c**) $I_{\text{app}} > I_{\text{Hc}}$. Perturbations from rest that lie in the *starred region* shown in (**c**) will approach the stable limit cycles

where I_{Hc} is the current at which there is a saddle–homoclinic orbit. The frequency T^{-1} approaches zero much more rapidly than in the SNIC case.

Figure 3.8 shows the phase plane for the membrane model near the critical current, I_{Hc}. There are three fixed points. The lower-left fixed point is always stable, the middle point is a saddle, and the upper-right point is an unstable spiral. For $I_{\text{app}} < I_{\text{Hc}}$ (Fig. 3.8a), the right branch of the unstable manifold of the saddle wraps around and returns to the stable fixed point. The upper branch of the stable manifold wraps around the spiral (in negative time). Note that the unstable manifold passes on the outside of the stable manifold. In Fig. 3.8b, the stable and unstable manifolds meet and form the homoclinic orbit at $I_{\text{app}} = I_{\text{Hc}}$. For $I_{\text{app}} > I_{\text{Hc}}$, the unstable manifold passes *inside* the stable manifold and wraps around a stable limit cycle. Thus, this model has a regime of bistability where there is a stable fixed point and a stable periodic orbit. Unlike the bistability in the Hopf case, the stable limit cycle does not surround the stable fixed point. In the Hopf case, an unstable periodic orbit acted to separate the stable fixed point from the stable limit cycle. For the present set of parameters, the stable manifold of the middle fixed point separates the two stable states. To get onto the limit cycle, it is necessary to perturb the potential into

the starred region in Fig. 3.8c. Consider a brief current pulse which perturbs the voltage. If this pulse is weak, then the system returns to rest. If it is very strong and passes the starred region, then the model will generate a single spike and return to rest. However, for intermediate stimuli (like the baby bear's porridge – just right), the system will settle onto the stable limit cycle.

Finally, we look closely at the bifurcation diagram (Fig. 3.7b). Near $I_{\text{app}} = 37$, there are two stable fixed points as well as a stable limit cycle. Thus, the model is actually "tristable." The reader is urged to explore this aspect of the model more carefully as an exercise.

3.4.4 Class I and Class II

The Morris–Lecar model illustrates several important features of neuronal firing. Three different mechanisms for switching from rest to repetitive firing were illustrated. In particular, the most common mechanisms are through the Hopf and SNIC bifurcations. In the 1940s, Hodgkin classified three types of axons according to their properties. He called these classes I and II, with class III being somewhere in-between the first two classes which we describe:

Class I. Axons have sharp thresholds, can have long latency to firing, and can fire at arbitrarily low frequencies.

Class II. Axons have variable thresholds, short latency, and a positive minimal frequency.

From this description, we can see that these two classes fall neatly into the dynamics of the SNIC and the Hopf bifurcations, respectively. Rinzel and Ermentrout [230] were the first to note this connection. Now there are many papers which classify membrane properties as class I or class II and mean SNIC and Hopf bifurcation dynamics, respectively.

Tateno et al. [259] have characterized regular spiking neurons (excitatory) and fast spiking neurons (inhibitory) in rat somatosensory cortex using this classification. (Note that many authors call the dynamics type I and type II instead of class I and class II.) Figure 3.9 shows some properties of cortical neurons. Regular spiking neurons appear to be class I; the minimal frequency is close to zero. Note that regular spiking neurons do not seem to have subthreshold oscillations (not shown). In contrast, fast spiking neurons appear to be class II; they have a minimum frequency of around 15 Hz. They also exhibit subthreshold oscillations. Near the critical current, they seem to switch back and forth between rest and firing. This suggests the possibility of a narrow range of bistability consistent with the subcritical Hopf bifurcation.

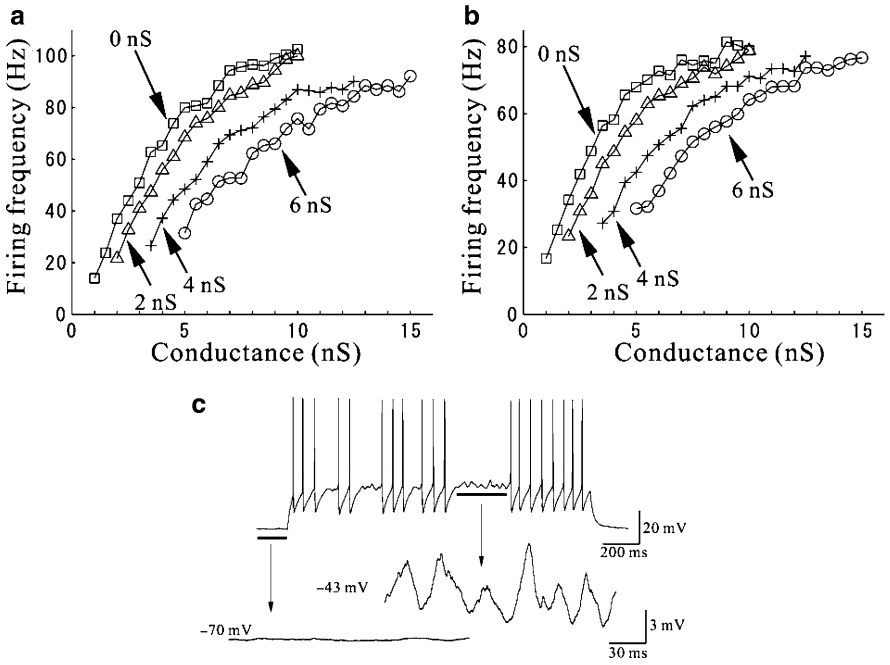

Fig. 3.9 Properties of regular spiking and fast spiking neurons in cortex. (**a**) Firing rate versus the AMPA receptor-type conductance for regular spiking neurons. Each curve represents a different level of GABA-type conductance. [Note that these cells have spike-frequency adaptation, so the interspike interval is not constant. Thus, this shows the interspike interval after several spikes as well as the steady state.] (**b**) Same as (**a**) for fast spiking neurons. (**c**) Mixture of spikes and subthreshold oscillations near the critical current for fast spiking neurons. (From [259])

3.5 Bifurcation Analysis of the Hodgkin–Huxley Equations

We now consider the space-clamped Hodgkin–Huxley model (1.43). In Chap. 2, we discussed the response to a brief current pulse. Figure 1.13 shows the effects of a brief current pulse at amplitudes ranging from 1 to 5 μA/cm^2. There appears to be a very sharp transition between an action potential and a minimal response. A constant current can induce the membrane to oscillate repeatedly as seen in the right panel in Fig. 1.13.

We can get a more global picture of the dynamics of the equations by looking at a bifurcation diagram. Figure 3.10a shows the behavior of the voltage as a function of the applied current, I_{app}. Lines represent fixed points and circles represent periodic orbits. The frequency of the oscillations is shown in Fig. 3.10c. The range is from about 40 Hz to about 150 Hz.

Note that there is a unique equilibrium point for all I_{app}. At $I_{\text{app}} \approx 10$, the resting state loses stability at a Hopf bifurcation. At a large value of $I_{\text{app}} \approx 154$ there is another Hopf bifurcation. From the figure, it seems clear that the bifurcation

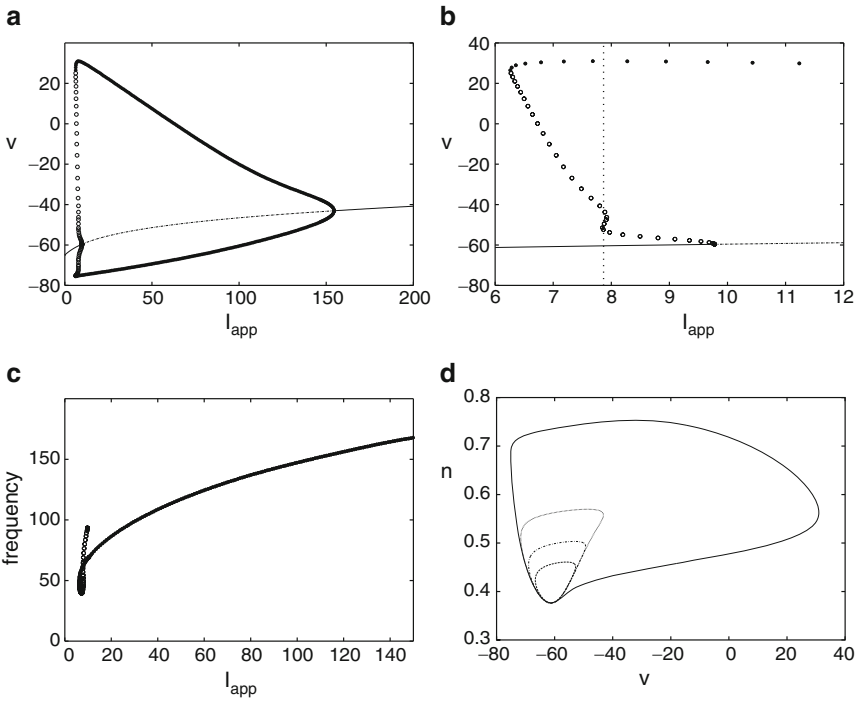

Fig. 3.10 Bifurcation diagram for the Hodgkin–Huxley model. (**a**) V versus I_{app}, the applied current. (**b**) Expanded view of (**a**). (**c**) Frequency as a function of current. (**d**) (V, n)-phase plane projection showing four different limit cycles

is subcritical at the low current and supercritical at the high current. At the lower Hopf bifurcation, there is a subcritical branch of unstable periodic orbits. Hence, the transition from resting behavior to oscillations is class II.

Figure 3.10b shows a blowup of the region near this Hopf bifurcation. Evidently, there are values of I_{app} near 7.88 where there are *four* different limit cycles. Figure 3.10d shows the projection of these limit cycles in the (V, n)-plane. Guckenheimer and Oliva [112] provide convincing numerical evidence for chaotic behavior near this lower current value. The chaos that they compute is *unstable*, so it will not be observed in simulations. For large values of current, the resting state stabilizes again through a supercritical Hopf bifurcation.

The apparent fact that there is a unique equilibrium point for all I_{app} has never been rigorously proved for the Hodgkin–Huxley equations. At equilibrium, each of the gating variables m, n, and h can be written as a function of V, so we find

$$\begin{aligned} I_{app} &= \bar{g}_L(V - E_L) + \bar{g}_{Na} m_\infty^3(V) h_\infty(V)(V - E_{Na}) \\ &\quad + \bar{g}_K n_\infty^4(V)(V - E_K) \equiv F(V). \end{aligned} \tag{3.3}$$

The statement that there is a unique equilibrium is a statement that $F(V)$ is monotonic for all V. Since this monotonicity depends very much on the details of the steady-state gate functions, it is not likely that any general theory of the monotonicity of F exists. We leave it as an exercise to show that if $|V|$ is large enough, then there is a unique value of I_{app} for which there exists an equilibrium.

If we assume the function $F(V)$ is monotonic, then it is possible to rigorously prove the existence of the two Hopf bifurcation points. Troy [272] proved under fairly general assumptions that there are two values of I_{app} at which the resting state loses stability at a pair of imaginary eigenvalues. Thus, from the Hopf bifurcation theorem, he was able to conclude that there is a branch of periodic solutions emerging from the fixed points. A rigorous proof of the direction of the bifurcation remains an open question.

Troy's proof relies on an analysis of the linearized equations and application of Hurwitz's criteria to the characteristic polynomial. We can sketch out some of the details. Troy's assumption that the function $F(V)$ is monotonic implies that for each I_{app} there is a unique V that satisfies (3.3). Furthermore, this implies that there are never any zero eigenvalues of the linear system. The linearization about the fixed point leads to a matrix with a very special form. It is zero except along the diagonal, across the first row, and down the first column:

$$M = \begin{pmatrix} -F_V & -F_m & -F_h & -F_n \\ \phi m'_\infty/\tau_m & -\phi/\tau_m & 0 & 0 \\ \phi h'_\infty/\tau_h & 0 & -\phi/\tau_h & 0 \\ \phi n'_\infty/\tau_n & 0 & 0 & -\phi/\tau_n \end{pmatrix}.$$

The characteristic polynomial for such matrices (which are called *mammillary* because they resemble a mammal with many suckling babies; here the voltage is the mother and the gates are the babies) is easy to compute and the result is a fourth-order polynomial of the form

$$P_M(\lambda) = \lambda^4 + a_3\lambda^3 + a_2\lambda^2 + a_1\lambda + a_0.$$

The coefficients are messy, but straightforward to compute. The Hopf bifurcation occurs when there are purely imaginary roots. The Routh–Hurwitz criterion provides the simplest test for this condition (see the digression that follows). For a fourth-order polynomial, there will be a Hopf bifurcation if $a_0 > 0$, $a_3 > 0$, $a_3a_2 - a_1 > 0$, and $R \equiv a_3a_2a_1 - a_1^2 - a_3^2a_0$ vanishes. Thus, Troy used assumptions for the shapes of the gating functions to prove there is a Hopf bifurcation by showing that the quantity R changes sign.

Digression: The Routh–Hurwitz Criterion

Consider the polynomial

$$P(\lambda) = \lambda^n + a_{n-1}\lambda^{n-1} + \cdots + a_1\lambda + a_0. \tag{3.4}$$

The Routh–Hurwitz determinants provide a simple way to tell if the real parts of the roots of P are negative. We define $a_n = 1$ and $a_j = 0$ for $j > n$ or for $j < 0$. We will form a series of matrices containing the coefficients a_j:

$$H_1 = a_{n-1},$$
$$H_2 = \begin{bmatrix} a_{n-1} & 1 \\ a_{n-3} & a_{n-2} \end{bmatrix},$$
$$H_3 = \begin{bmatrix} a_{n-1} & 1 & 0 \\ a_{n-3} & a_{n-2} & a_{n-1} \\ a_{n-5} & a_{n-4} & a_{n-3} \end{bmatrix},$$

and so on up to H_n. Each matrix is square and the first column contains every other coefficient, $a_{n-1}, a_{n-3}, \ldots$. The roots of $P(\lambda)$ have negative real parts if and only if $\det H_j > 0$ for $j = 1, \ldots, n$. For example:

$n = 1$. $a_0 > 0$
$n = 2$. $a_0 > 0$ and $a_1 > 0$
$n = 3$. $a_0 > 0, a_2 > 0, a_1 a_2 - a_0 > 0$
$n = 4$. $a_0 > 0, a_3 > 0, a_3 a_2 - a_1 > 0, a_3 a_2 a_1 - a_1^2 - a_3^2 a_0 > 0$

We note the following:

- $\det H_n = a_0 \det H_{n-1}$, so this means $a_0 > 0$ is necessary. If $a_0 = 0$, then there is a zero eigenvalue.
- If $\det H_{n-1} = 0, a_0 > 0$, and $\det H_j > 0$ for $j < n-1$, then there are imaginary roots.

These two criteria allow us to determine where possible saddle–node (eigenvalue 0) and Hopf (imaginary eigenvalues) bifurcations occur.

End of digression

3.6 Reduction of the Hodgkin–Huxley Model to a Two-Variable Model

We have seen that two-dimensional models, such as the Morris–Lecar equations, exhibit many important features of the more complicated Hodgkin–Huxley equations. The Morris–Lecar equations generate action potentials, there is a threshold for firing, and, depending on parameters, there are several mechanisms for the generation of oscillatory behavior. In this section, we shall describe two ways in which dynamical systems methods can be used to formally reduce the four-dimensional Hodgkin–Huxley model to a two-dimensional system of equations. Reduction methods will be very useful in later sections when we consider networks of neurons.

Rinzel [226] developed a simple method based on two observations. The first is that $\tau_m(V)$, the voltage-dependent time constant for the gating variable m, is much

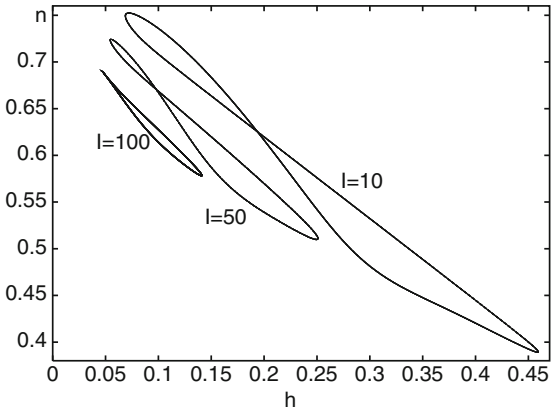

Fig. 3.11 Projection of limit cycles in Hodgkin–Huxley equations in the (n, h)-plane

smaller than both τ_h and τ_n. Because τ_m is small, $m(t)$ is very close to $m_\infty(V(t))$. If we replace m by $m_\infty(V)$ in the voltage equation, then this reduces the Hodgkin–Huxley model by one equation. The second observation, first made by Krinskii and Kokoz [164], is that $(n(t), h(t))$ lies nearly along a line $n = b - rh$, where b and r are constants. Figure 3.11 shows these curves at three different currents. The slope and the intercept depend somewhat on the current, but Rinzel ignored this. Hence, we replace n by $b - rh$ in the voltage equation and obtain the reduction to a two-dimensional model. We leave the analysis of this model as an exercise.

A common method for comparing parameters which have different units is to render the model in terms of dimensionless variables. Kepler et al. [150] described a method for comparing the timescales of all the gating variables. Each voltage-dependent gate $x(t)$ satisfies an equation of the form

$$x' = (x_\infty(V) - x)/\tau_x(V).$$

The functions $x_\infty(V)$ are monotonic, so they are invertible. Thus, Kepler et al. introduced a new variable V_x for each gate, where $x(t) = x_\infty(V_x(t))$. They obtained an equivalent dynamical system, but now every variable has the dimensions of voltage. The equivalent potentials satisfy

$$\frac{\mathrm{d}V_x}{\mathrm{d}t} = \frac{x_\infty(V) - x_\infty(V_x)}{\tau_x(V)x'_\infty(V_x)},$$

where $x'_\infty(V_x)$ is the derivative of x_∞ with respect to V. Now, we must simulate the equations in these new variables and this allows us to compare the amplitudes and the time courses of the responses of all the variables. Figure 3.12a shows a plot of the equivalent potentials for the four-variable Hodgkin–Huxley equations. From the figure, it looks as if V_m and V have roughly the same temporal dynamics, whereas

V_h and V_n have similar time courses. Thus, we create a reduced model by setting $V_m = V$ and $V_n = V_h$. There are two possible reduced models: use the dynamics of V_h and set $n = n_\infty(V_h)$ or use the dynamics of V_n and set $h = h_\infty(V_n)$. We leave the latter case to the reader and consider the (V, V_h) system.

The two-dimensional (V, V_h) system has the following form:

$$\begin{aligned} c_{\mathrm{M}} \frac{\mathrm{d}V}{\mathrm{d}t} &= I_{\mathrm{app}} - \bar{g}_{\mathrm{Na}} m_\infty^3(V) \bar{h}_\infty(V_h)(V - E_{\mathrm{Na}}) \\ &\quad - \bar{g}_{\mathrm{K}} n_\infty^4(V_h)(V - E_{\mathrm{K}}) - g_{\mathrm{L}}(V - E_{\mathrm{L}}), \\ \frac{\mathrm{d}V_h}{\mathrm{d}t} &= \frac{h_\infty(V) - h_\infty(V_h)}{\bar{\tau}_h(V, V_h)}, \end{aligned}$$

where $\bar{\tau}_h$ is the effective time constant, $\tau_h(V) h'_\infty(V_h)$. Figure 3.12b shows the bifurcation diagram for the reduced system. It cannot have any more fixed points than the full system since both have identical equilibria. There is a subcritical Hopf bifurcation at roughly $I_{\mathrm{app}} = 6.8$ which is slightly lower than that for the original Hodgkin–Huxley equations. What is strikingly different is that the reduced model continues to oscillate at an extremely large applied current. The second Hopf bifurcation does not occur until $I_{\mathrm{app}} = 267$, much higher than in the original

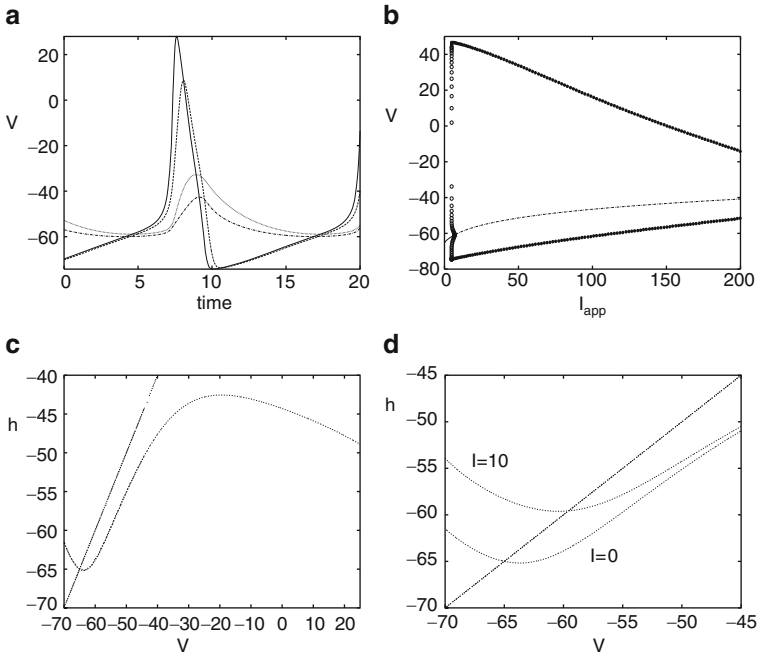

Fig. 3.12 Equivalent potentials for the Hodgkin–Huxley model. (**a**) The voltages of the four variables. (**b**) Bifurcation diagram for the (V, V_h) system, (**c**) Phase plane at rest. (**d**) Phase plane showing how the fixed point moves to the middle branch as I_{app} increases

four-variable system. The phase plane is shown for $I_{\text{app}} = 0$ in Fig. 3.12c. A convenient aspect of the equivalent potential method is that the V_h-nullcline is just $V = V_h$. The V-nullcline has a cubic form which is typical in many neural models and absolutely necessary to get oscillations.

3.7 FitzHugh–Nagumo Equations

The simplified (V, n) version of the Hodgkin–Huxley equations and the Morris–Lecar equations share a common feature insofar as their nullclines are concerned. The V-nullcline has a cubic shape, whereas the recovery nullcline is a monotonically increasing function of the voltage. In 1961, FitzHugh [89] developed a simplified model which captures the essence of the cubic nature of the V-nullcline and has many of the properties of the more complicated models that we have already discussed. Because of its pivotal importance in the literature (particularly, the mathematical literature), we discuss it briefly at this point. We leave as an exercise the numerical and qualitative analysis of these equations. The equations (called the FHN equations) have the form

$$\frac{\mathrm{d}V}{\mathrm{d}t} = V(V-a)(1-V) - w + I, \tag{3.5}$$

$$\frac{\mathrm{d}w}{\mathrm{d}t} = \epsilon(V - \gamma w), \tag{3.6}$$

where $0 < a < 1$, $\epsilon > 0$, and $\gamma \geq 0$. The actual model is based on a modification of the van der Pol equation:

$$C\frac{\mathrm{d}V}{\mathrm{d}t} + F(V) + J = 0,$$

$$L\frac{\mathrm{d}J}{\mathrm{d}t} = V.$$

The van der Pol equation arises from an electrical circuit with a linear capacitor, linear inductor, and nonlinear resistor in parallel. C is the capacitance, L the inductance, $F(V)$ a nonlinear current depending on the voltage, V, across the capacitor, and J the current through the inductor. By adding a driving current and the additional $-\gamma w$, FitzHugh created a model for the action potential. At about the same time, Nagumo and colleagues developed a similar model.

The FHN equations have been used to model many physiological systems from nerve to heart to muscle and is a favorite model for the study of excitability. In most applications, ϵ is small, so the recovery variable is much slower than the voltage. When $I = 0$ and γ is small enough, there is a unique fixed point at the origin. As I increases, this fixed point becomes unstable through a Hopf bifurcation and a limit cycle emerges. We will provide an extensive exercise later for examining the behavior of this popular and much studied model.

3.8 Bibliography

An excellent reference for an introduction to dynamical systems is Strogatz [255]. More advanced textbooks include those of Guckenheimer and Holmes [111], Perko [212], and Kuznetsov [167]. FitzHugh [89] was perhaps the first to use phase plane analysis to study the Hodgkin–Huxley and reduced models. Much of the analysis in this chapter builds on the paper by Rinzel and Ermentrout [230], who carefully described geometric methods, including phase planes and bifurcation theory, applied to reduced neuronal models. They also recognized the relationship between class I and class II excitability and the geometric properties of different types of bifurcations. Izhikevich [135] covers most of the material described in this chapter, but in more detail.

3.9 Exercises

There are a number of exercises on simplified neural models which are popular in the literature. Rather than discussing these in the text, we have chosen to leave them as an extended set of exercises. In later chapters, we will refer to these models and their properties. Thus, it would be a good idea to do those related to the leaky integrate and fire and quadratic integrate and fire models.

1. Show that the gating functions used by Morris and Lecar are derived from the Boltzmann model.
2. Near rest, the potential of the Morris–Lecar system can be approximated by its linearization:
$$C_{\mathrm{M}}\frac{\mathrm{d}V}{\mathrm{d}t} = I(t) - aC_{\mathrm{M}}(V - V_{\mathrm{R}}),$$
where a is as computed above. Suppose I is a square pulse of current with duration T and magnitude I_0. Estimate the value of I_0 needed to evoke an action potential assuming that one will occur if V crosses V_t (see Fig. 3.3). Sketch the critical value I_0 as a function of T. This is called the *strength–duration curve*. The minimum strength needed to elicit a response is called the *rheobase* and the stimulus duration needed to elicit an action potential when the stimulus is twice the strength of the rheobase is called the *chronaxie*. Compute the rheobase and chronaxie using this estimate. Numerically determine them as well.
3. Simulate the Morris–Lecar model with the homoclinic parameters and $I = 36$ corresponding the phase plane in Fig. 3.8c. (a) Starting at rest, give a 5-ms current pulse sufficient to produce a single spike. Weaken the current pulse to perturb the model to the stable limit cycle. (b) Set $I = 38$. This corresponds to the vertical line in Fig. 3.7b where there is tristability. Starting at rest, is it possible to inject a single pulse of current to get the system to go from the lower resting state to the upper resting state? If not, figure out a stimulation sequence that will let you go from rest to the upper state.

4. *Exploring the FHN model I.* The fixed points of this model satisfy $w = V/\gamma$ and $I = V/\gamma - V(V-a)(1-V) \equiv h(V)$. The latter is a cubic. It can have at most three roots. Differentiating $h(V)$ and setting this to zero allows us to find local maxima and minima. (a) Find these as a function of a and γ. Show that $\gamma > 3/(1-a+a^2) \equiv \gamma^*(a)$ for such extrema to exist. Next, set V to these roots and use this to find values of I where there are saddle–node bifurcations. This summarizes the steady-state behavior of the model. (b) Consider the case when $\gamma < \gamma^*(a)$ so that there is only a single root. Since there is one root, there can be no bifurcation at a zero eigenvalue as I varies. Thus, the only way to lose stability is a Hopf bifurcation. Show that the trace of the linearization is

$$T = -3V^2 + (2+a)V - a - \epsilon.$$

   Show that there are two values of V such that the trace vanishes as long as $3\epsilon < a^2 - a + 1$. These correspond to two distinct values of current ($I = h(V)$) at which there is a Hopf bifurcation.
5. *Exploring the FHN model II.* (a) Choose $\epsilon = 0.02$, $\gamma = 1$, and $a = 0.1$. For $I = 0$ show that the system is excitable, that is, show that there is an action potential if the voltage is taken sufficiently past threshold. (b) Compute the bifurcation diagram and look at the frequency–current plot. Notice that the bifurcation is nearly vertical. Compute several limit cycles along the nearly vertical branch. Notice how they hug the middle branch of the nullcline. This is an example of a phenomenon called a *canard* and is common in systems with a small parameter (e.g., ϵ).
6. *The integrate and fire model.* A classic approximation for the firing of a cell is the leaky integrate and fire model [174]. This model has the form

$$\tau \frac{\mathrm{d}V}{\mathrm{d}t} = -(V - V_{\mathrm{R}}) + R_{\mathrm{M}} I, \tag{3.7}$$

   where R_{M} is the membrane resistance, τ the time constant, and V_{R} the resting potential. In addition to this linear equation, there is a nonlinear reset condition. If $V(t^-) = V_{\mathrm{spike}}$, then an action potential occurs and $V(t)$ is reset to V_{reset}. In many cases, an additional condition is imposed in which V is prevented from firing for a period, T_{ref}, the "refractory" period. Assume $V_{\mathrm{R}} < V_{\mathrm{spike}}$ and $V_{\mathrm{reset}} < V_{\mathrm{spike}}$. Find the critical value of I, I_{min}, under which the leaky integrate and fire model fires repetitively. Compute the F–I curve; the firing rate as a function of the applied current for $I > I_{\mathrm{min}}$. Show that for large values of I, the firing rate is linear with respect to I when $T_{\mathrm{ref}} = 0$.
7. *Spike response model.* Consider the leaky integrate and fire model with a time-dependent current, $I(t)$:

$$\tau \frac{\mathrm{d}V}{\mathrm{d}t} = I(t) - V(t) - A \sum_j \delta(t - t_j),$$

where $A = \tau(V_{\text{spike}} - V_{\text{reset}})$. We have formally included the reset into the equations by adding the delta function term. The values t_j are the times for which $V(t)$ crosses V_{spike} from below; that is, the spike times. Integrate this equation to convert it to the following form:

$$V(t) = V(0)\mathrm{e}^{-t/\tau} + \sum_j \eta(t - t_j) + \int_0^t k(t-s)I(s)\mathrm{d}s,$$

where

$$\eta(t) = H(t)(V_{\text{reset}} - V_{\text{spike}})\mathrm{e}^{-t/\tau}$$

and

$$k(t) = \frac{1}{\tau}\mathrm{e}^{-t/\tau}.$$

Here, H is the Heaviside step function. Gerstner et al. [99] considered classes of models like this where η takes a more general form. These models are called *spike response models.* For example, $\eta(t)$ could include an additional spike frequency adaptation term, for example,

$$\eta(t) = H(t)[k_1\mathrm{e}^{-t/\tau} + k_2\mathrm{e}^{-t/\tau_a}].$$

Unfortunately, once these extra terms are added, it becomes difficult to compute even the steady-state firing rate. Later in the book, we will use this formulation to compute the velocity of waves in networks of coupled integrate and fire models.

8. In the Morris–Lecar model with class I dynamics (the SNIC), the potential near the bifurcation satisfies the following differential equation:

$$\frac{\mathrm{d}V}{\mathrm{d}t} = a(I - I_{\text{SN}}) + b(V - V_{\text{SN}})^2, \tag{3.8}$$

where a and b are positive numbers that can be determined from the actual dynamics (see [167]). (What are the physical dimensions of a, b?) This is called the *quadratic integrate and fire* model. (a) By integrating this equation, show that V can go to infinity in finite time. When $V(t)$ goes to infinity, we say that a spike has been generated. (b) Suppose $I < I_{\text{SN}}$ and find the fixed points for this, V_{rest} and V_{thr}, corresponding to the stable and unstable fixed points,

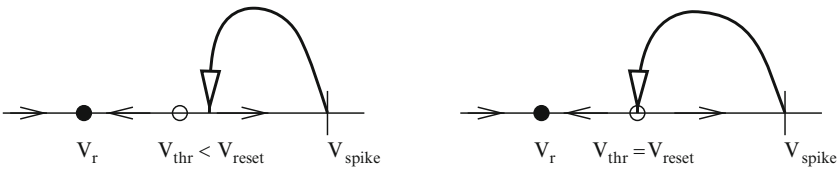

respectively. Suppose $V(0) > V_{\text{thr}}$. Compute the time to spiking as a function of $V(0) - V_{\text{thr}}$. (c) Show that if $I > I_{\text{SN}}$, then $V(t)$ goes to infinity no matter what the initial condition is. In particular, compute the time it takes to reach infinity if $V(0) = -\infty$. (d) Let

$$V(t) = V_{\text{SN}} + \frac{c}{b}\tan(\theta/2).$$

where c^{-1} has dimensions of time. Show that $\theta(t)$ satisfies

$$\frac{\mathrm{d}\theta}{\mathrm{d}t} = c(1-\cos\theta) + \frac{ab}{c}(1+\cos\theta)[I - I_{\text{SN}}]. \tag{3.9}$$

This is called the *theta model*. Ermentrout and Kopell [72] showed that this was the normal form for a system near a saddle–node limit cycle bifurcation. Sketch the phase line for this when $I < I_{\text{SN}}$, $I = I_{\text{SN}}$, and $I > I_{\text{SN}}$. Compute the F–I curve when $c = 1$.

9. A variant of the quadratic integrate and fire model truncates the spike and the reset. [175] first suggested the model

$$\tau\frac{\mathrm{d}V}{\mathrm{d}t} = a(V - V_{\text{R}})(V - V_{\text{thr}}) + R_{\text{M}}I \tag{3.10}$$

with the condition that if $V(t) = V_{\text{spike}} > V_{\text{thr}}$, then $V(t)$ is reset to V_{reset}. When $I = 0$, V_{r} is the resting state and V_{thr} is the threshold. If $V(0) > V_{\text{thr}}$, then the model will spike. (a) Compute the F–I curve for this model. Note that it is somewhat different from the quadratic integrate and fire in (3.8) owing to the finite reset.
(b) Suppose $V_{\text{reset}} > V_{\text{thr}}$. Then, this model is bistable for $I = 0$ or I is sufficiently small and has a fixed point near V_{r} and a periodic solution. As $V_{\text{reset}} \to V_{\text{thr}}^{+}$, the period goes to infinity and this model has the equivalent of a homoclinic orbit. (see the diagram above.) Compute the period as a function of $V_{\text{reset}} - V_{\text{thr}}$. (c) Now suppose $V_{\text{R}} < V_{\text{reset}} < V_{\text{thr}}$. As I increases, either the stable resting state will reach V_{reset} from below or the unstable fixed point will reach V_{reset} from above and form a homoclinic. Find conditions for the latter scenario and sketch the bifurcation diagram as I varies. Compare this with the diagram for the Morris–Lecar model in parameter set 3. From this exercise, it should be clear that the quadratic integrate and fire model has much richer dynamics than the leaky integrate and fire model precisely because it has a true spiking threshold which is different from the value of the actual spike.
10. Karbowski and Kopell [145] introduced a linear model:

$$\tau\frac{\mathrm{d}V}{\mathrm{d}t} = R_{\text{M}}I + a|V|, \tag{3.11}$$

where $a > 0$ is parameter. (a) Show that this is qualitatively like (3.10). How does the firing rate scale near $I = 0$? (b) One can define a class of scalar neural models by considering

$$\tau \frac{\mathrm{d}V}{\mathrm{d}t} = R_{\mathrm{M}} I + f(V).$$

Suppose $f(V) = |V|^p$, where $p > 1$. The model spikes when $V(t)$ reaches infinity, in which case the neuron is reset to negative infinity. What is the firing rate of such a neuron for I large? That is, how does it scale with p? For example, we know that when $p = 2$, the firing rate scales like the square root of I.

11. A class of models related to the theta model are called *ring* models [75, 291]. These are models for excitable activity which lies on the unit circle:

$$\frac{\mathrm{d}x}{\mathrm{d}t} = f(x) + I,$$

where $f(x + 2\pi) = f(x)$ is a bounded periodic function. For certain ranges of I, the system has two fixed points: a saddle and a node. The saddle point acts as a threshold. Since $f(x)$ is bounded, for I large enough, there are periodic solutions to the equation and thus there is repetitive firing. Suppose $f(x)$ is $C^2[0, 2\pi)$ and periodic. Write an expression for the period of the oscillations when there is repetitive firing. Discuss the mechanism from going from a stable resting state to repetitive firing. Can there ever be bistability?

12. Fourcaud et al. [91] introduced the exponential integrate and fire model:

$$C \frac{\mathrm{d}V}{\mathrm{d}t} = -g_{\mathrm{L}}(V - V_{\mathrm{L}}) + a \exp(bV) + I.$$

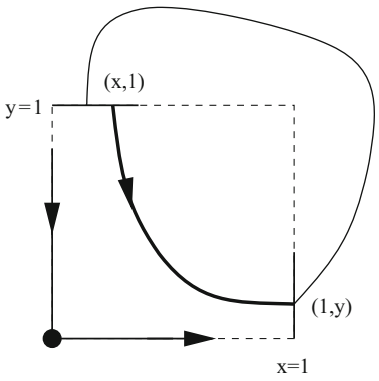

Set $g_L = 0$ and assume a, b, and C are positive. Find an expression for the firing rate as a function of I in terms of an integral. Show that if a and b are positive, then for I large enough, the solution of the ordinary differential equation blows up in finite time. Obtain an estimate for how fast it blows up by ignoring the linear terms, $g_{\mathrm{L}}(V - E_{\mathrm{L}})$. That is, the blowup time is roughly

$$\int_0^{\infty} \frac{\mathrm{d}V}{I + a\exp(bV)}.$$

Evaluate this as a function of I.

13. *Period near a homoclinic*. This is actually an exercise in dynamical systems, but is instructive in that it shows the period of the homoclinic orbit. Assume the origin is a saddle point with eigenvalues $-\mu$ and ν, the y-axis is the stable manifold, and the x-axis is the unstable manifold. Moreover, $\mu > \nu > 0$. Consider a point $(1, y)$ on the little interval at $x = 1$. This is mapped onto the little interval at $y = 1$, via $(1, y) \to (ay + b, 1)$. The parameter a is positive and will not really matter. The parameter b is the distance from the homoclinic orbit. Note that if $b = 0$, then $(1, 0) \to (0, 1)$ is the homoclinic orbit. Starting at $(x_0, 1)$, we follow the linear dynamics

$$x' = \nu x; \quad y' = -\mu y.$$

This maps the $y = 1$ interval onto the $x = 1$ interval. Thus, we obtain a map from $(1, y_{\mathrm{old}}) \to (1, y_{\mathrm{new}})$. (a) Show that the map of the y values is

$$y_{\mathrm{new}} = (a y_{\mathrm{old}} + b)^r,$$

where $r = \mu/\nu > 1$. For b sufficiently small, show that $y = b^r + o(b^r)$ is a fixed point. Show that the fixed point is stable. (b) Since the map from $x = 1$ to $y = 1$ is instant, the period is the time it takes to go from $y = 1$ to $x = 1$. Show that at the fixed point

$$T \sim -\frac{1}{\nu} \log b.$$

(Note: This relies on the fact that $r > 1$. If $r < 1$, then the fixed point will be unstable and so the periodic orbit will also be unstable.)